frontiers | Frontiers in Energy Research

TYPE Original Research
PUBLISHED 07 December 2023
DOI 10.3389/fenrg.2023.1325405

OPEN ACCESS

EDITED BY
Qian Chen,
Tsinghua University, China

REVIEWED BY
Mamdouh El Haj Assad,
University of Sharjah, United Arab Emirates
Atul Sharma,
Rajiv Gandhi Institute of Petroleum Technology, India

*CORRESPONDENCE
Zehui Chang,
changzehui@163.com

RECEIVED 21 October 2023
ACCEPTED 27 November 2023
PUBLISHED 07 December 2023

CITATION
Yang J, Chang Z, Zhang X and Zhu G (2023), Performance investigation and mass transfer enhancement of a novel cone-type solar seawater still. *Front. Energy Res.* 11:1325405. doi: 10.3389/fenrg.2023.1325405

Performance investigation and mass transfer enhancement of a novel cone-type solar seawater still

Jie Yang[1,2], Zehui Chang[1,3]*, Xin Zhang[1] and Guopeng Zhu[1]

[1]College of Energy and Power Engineering, Inner Mongolia University of Technology, Hohhot, China, [2]Department of Physics, Luliang University, Luliang, China, [3]Engineering Center of Solar Energy Utilization Technology, Inner Mongolia University of Technology, Hohhot, China

There are some disadvantages in the operating process of the basin solar seawater still (BSSS), such as long mass transfer distance, large heat indolence, huge floor space, and poor bearing pressure ability. A novel cone-type solar seawater still (CTSSS) is presented to overcome the weaknesses of the BSSS in this study. The CTSSS has the characteristics of seawater liquid film evaporation, short mass transfer distance, the condensation sleeve is parallel to and above the evaporation sleeve, and the condensation area is larger than the evaporation area. In order to clarify the performance of the CTSSS, the influence mechanism of feed seawater mass flow rate, heating power and heating temperature on the fresh water yield of the CTSSS was analyzed, the method of enhancing the mass transfer of the binary mixed gas in the CTSSS was explored, and the law of heat and mass transfer of the binary mixed gas in the annular enclosed small space was investigated. The results indicated that the maximum fresh water yield of the CTSSS is 62.7 g/20 min at the feed seawater mass flow rate of 400 g/h when the input power is 200 W, which is 4.5% higher than that when the feed seawater mass flow rate is 300 g/h. The performance ratio (*PR*) of the CTSSS is increased as the heating power, the *PR* of the CTSSS is 0.65 when 180 W heating power is employed. The steady state fresh water yield of the CTSSS with mirror condensation sleeve at 85°C is 84.6 g/20 min, which is 12.1% higher than that with non-mirror condensation sleeve Compared with the CTSSS with non-mirror condensation sleeve, the value of proportions of radiative heat transfer in the total heat transfer of the CTSSS with mirror condensation sleeve decreased by 6.6%, and the value of proportions of evaporative heat transfer increased by 6.4%. This study would provide a reference for small-scale decentralized application of solar desalination in remote areas.

KEYWORDS

cone-type, solar, seawater desalination, mass transfer, mirror condensation

1 Introduction

Fresh water is vital to human development for it is necessary for human survival and social production. However, the human demand for fresh water is increasing with the expansion of the global population and the development of industry and agriculture, which has led to the shortage of fresh water. What is more serious is that the fresh water crisis has become the third-largest crisis of human beings (Abou-Shady and El-Araby, 2022). It is predicted that 6 billion people will live in countries or regions with fresh water shortages by

2050 (Wang and Huo, 2022; Wang et al., 2023). Seawater desalination is one of the best ways to solve the water shortage problem (Yang et al., 2023). However, the high energy consumption of seawater desalination has limited its development, even though the raw water comes from abundant seawater. Fortunately, the areas where fresh water resources are in short supply are those with abundant solar energy and seawater resources. Solar energy is a renewable energy with huge reserves and wide distribution (Arunkumar et al., 2021), so its use for seawater desalination has broad application prospects (Srithar and Rajaseenivasan, 2018).

As a small size device for desalination, solar seawater still has the advantages of simple structure, low price, and easy maintenance. It is especially suitable for small-scale decentralized applications of solar desalination in remote areas. Solar seawater stills are divided into the basin solar seawater still (BSSS) and the tubular solar seawater still (TSSS) (Ahmed et al., 2021a). For both BSSS and TSSS, the application value depends on its fresh water yield performance. The methods to improve the fresh water yield of the BSSS and TSSS include adding a solar concentrator (Choong et al., 2020), designing a multi-stage still (Yeang et al., 2023), increasing the evaporation area by adding sand troughs (Nagaraju et al., 2022), adding the nanofluids (Sangeetha et al., 2022), and so on. In a study by Tiwar (Tiwar, 1988), it is concluded that the daily fresh water yield and the purity of the fresh water from a horizontal tubular solar seawater still (HTSSS) are higher than that from a BSSS under the same condition. So much research has been committed to improving the fresh water yield performance of the HTSSS.

Kabeel et al. (2021) used v-corrugated absorbers and wick materials to improve the solar absorption efficiency and the evaporation rate of the HTSSS. The experimental results showed that the daily fresh water yield and daily efficiency of the still are 6,010 mL/(m^2·d) and 44.82%, which are 51.4% and 46.82% higher than that of the HTSSS with a flat absorber. Essa et al. (2021) designed a modified HTSSS to reduce the water depth of the HTSSS by a rotating drum, and results illustrated that the daily fresh water yield is 6,600 mL/(m^2·d), which is 175% higher than that of a traditional HTSSS. Ahmed et al. (2021b) installed a double-effect HTSSS on the focal line of a parabolic concentrator with a solar tracking system to improve its evaporation temperature and fresh water yield. The test in actual weather showed that the daily fresh water yield and daily efficiency of the still are 5.2 L/(m^2·d) and 40.4%, respectively. Yan et al. (2021) proposed a HTSSS that combines immersion cooling and vacuum operation. The experimental research showed that the fresh water yield and the performance ratio of the HTSSS under an operating pressure of 40 kPa are 9.8 kg/(m^2·d) and 1.87, respectively.

Additionally, heat storage materials and nanoparticles are also commonly used to improve the fresh water yield performance of solar stills (Jafaripour et al., 2023). Elashmawy et al. (2021) placed 12 aluminum tubes filled with phase change heat storage materials inside the water tank of the HTSSS with a parabolic solar concentrator. The outdoor tests showed that the daily fresh water yield of the still is 5.55 L/(m^2·d), and the daily efficiency is 44.1%. Sharshir et al. (2022) added carbon black nanoparticles in a HTSSS, and the results confirmed that the nanoparticles increased the daily fresh water yield of the still by 16.2%.

In order to shorten the mass transfer distance, Chang et al. (2015) proposed a vertical tubular solar seawater still (VTSSS), and committed experimental research on a three-effect VTSSS. The results showed that the performance ratio of the VTSSS is 1.89. Hou et al. (2018a) tested the effects of the wick materials thickness, the mass flow rate of the feed seawater, the operating pressure, and the cooling airflow rate on the VTSSS. The results revealed that the yield of the VTSSS is 248.0 g/h when the thickness of the wick materials is 1 mm and the mass flow rate of the feed seawater is 0.12 g/s. The fresh water yield of the VTSSS can be increased by 23.92% under negative pressure. Li et al. (2020) analyzed the effect of characteristic size on the fresh water yield performance of VTSSS. The experimental results showed that the fresh water yield per unit condensation area increased by 24.16%, and the steady state operating temperature increased by 7.21 °C with the characteristic size added from 15 mm to 35 mm. Hou et al. (2018b) investigated the effect of air, carbon dioxide, argon, nitrogen, oxygen, and helium on the fresh water yield of a three-effect VTSSS. It is found that the yield of the still is 1.19 kg/h when the heating temperature is 80°C and the carrier gas is helium, which is 30.76% higher than that when the carrier gas is air.

To further improve the fresh water yield performance of seawater still by reducing the mass transfer distance and

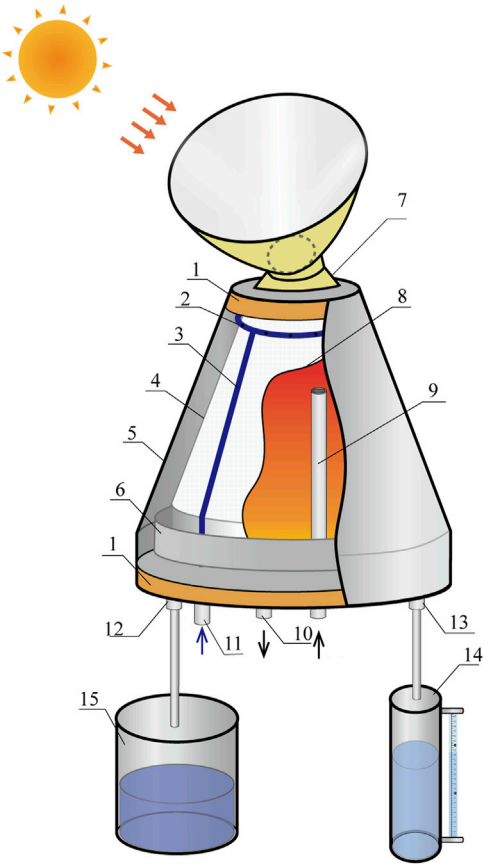

FIGURE 1
Schematic diagram of the CTSSS. 1–insulation layer, 2–perforated tube, 3–feed seawater pipe, 4–wick materials, 5–outer conical sleeve, 6–water linerboard, 7–solar collector, 8–inner conical sleeve, 9–inlet pipe, 10–outlet pipe, 11–feed seawater pipe entrance, 12–brine outlet pipe, 13–fresh water outlet pipe, 14–fresh water tank, 15–brine collection tank.

TABLE 1 Design specifications of the CTSSS.

Specification	Value	Material
Inner conical sleeve	Upper bottom diameter = 50 mm, lower bottom diameter = 404 mm, height = 386 mm, thickness = 1.2 mm	Stainless steel
Outer conical sleeve	Upper bottom diameter = 62 mm, lower bottom diameter = 460 mm, height = 396 mm, thickness = 1.2 mm	Stainless steel
Inlet pipe	Outer diameter = 20 mm, thickness = 2.5 mm, height = 367 mm	Stainless steel
Outlet pipe	Outer diameter = 20 mm, thickness = 2.5 mm, height = 60 mm	Stainless steel
Water linerboard	Diameter = 434 mm, thickness = 1.2 mm	Stainless steel
Fresh water tank	Outer diameter = 108 mm, thickness = 1.2 mm, height = 500 mm	Stainless steel
Brine collection tank	Outer diameter = 300 mm, thickness = 1.2 mm, height = 500 mm	Stainless steel

reinforcing the mass transfer rate of the binary mixed gas, this study proposes a CTSSS with the condensation surface and the evaporation surface inclined. The titled condensation surface can intercept and condense the water vapor from the evaporation surface. In this study, firstly, the heat and mass transfer process in the CTSSS was analyzed. Secondly, an experimental setup was developed to test fresh water yield performance of the CTSSS with different feed seawater mass flow rates, heating power and heating temperatures. Finally, the condensation sleeve of the CTSSS was replaced by a mirror condensation sleeve to enhance the fresh water yield performance. This work explores a novel method of small distributed solar seawater desalination.

2 Materials and methods

2.1 Structure parameters of the cone-type solar seawater still

The CTSSS proposed in this study is a conical structure, so its bearing pressure ability is strong and its floor space is small. It is suitable for small-scale decentralized application of solar desalination in remote areas for its advantages of easy processing and low manufacturing cost. The structure of the CTSSS is shown in Figure 1, and it is mainly composed of a solar collector and cone-type solar seawater still. The solar collector provides heat for the cone-type solar seawater still. The cone-type solar seawater still produces fresh water by heating the seawater liquid film and making it evaporate. The cone-type solar seawater still is mainly composed of two conical sleeves with different heights and diameters. The inner and outer conical sleeves are the evaporation surface and condensation surface, respectively. It is the heated water in the inner conical sleeve that provides heat for the seawater evaporation on the outer surface of it. Insulation layers are set at the top and bottom of the CTSSS to reduce heat loss. The design specifications of the CTSS are shown in Table 1. The distance between the evaporation surface and the condensation surface is 10 mm (the characteristic size of the CTSSS).

During operation, the solar collector gathers the solar rays and transmits them downward to the inside of the inner conical sleeve of the CTSSS, which is also the heating tank. The temperature of the heating water in the heating tank is increased as the solar rays are converted from radiant energy to heat energy. The seawater enters the perforated tube at the top of the inner conical sleeve through the feed seawater pipe. Then the seawater is absorbed by the wick materials attached to the inner conical sleeve and forms the seawater liquid film after flowing out from the outlet holes on the perforated tube. The seawater liquid film absorbs heat from the surface of the inner conical sleeve, and then its temperature rises and starts to evaporate. The water vapor evaporates from the seawater liquid film and condenses on the outer conical sleeve. Then it converts to fresh water and releases condensation latent heat. Eventually, the fresh water and the unevaporated brine flow into the fresh water tank and the brine collection tank under gravity, respectively.

The CTSSS has the following characteristics: ① The evaporation mode of the CTSSS is falling film evaporation, which is beneficial to form a uniform seawater liquid film on the evaporation surface, to reduce the heat energy consumption of generating the water vapor and to decrease the response time of the CTSSS. ② The evaporation surface and condensation surface are tilted and mutually parallel, and those can theoretically be infinitely close. The heat transfer distance of the binary mixed gas in the CTSSS is short. Meanwhile, the content of non-condensable gas in the CTSSS is less, which weakens the influence of non-condensable gas on heat and mass transfer and improves the fresh water yield in the same input heat per unit time. ③ The condensation surface is installed parallelly to and above the evaporation surface, and the condensation area is always larger than the evaporation area, which is conducive to the condensation of water vapor and the reduction of the vertical condensation temperature difference.

2.2 Experimental setup and procedure

The solar collector converts solar energy into heat energy to supply heat for the evaporation of water vapor during the operation. But it is difficult to make the CTSSS reach a steady state with solar energy because the energy supply of the solar collector is unstable under actual weather conditions. So the test was carried out in the laboratory where the ambient temperature and wind speed were stable, and the electric heating device was used instead of a solar collector to heat the CTSSS during the trial. The influence of the salt concentration of the feed seawater on the experiment was not considered, so seawater was replaced by tap water during the test.

The test system and the experimental device are shown in Figure 2. The system is mainly composed of the seawater tank, CTSSS, fresh water tank, brine collection tank, electronic transformer, digital data recording, and data processing system.

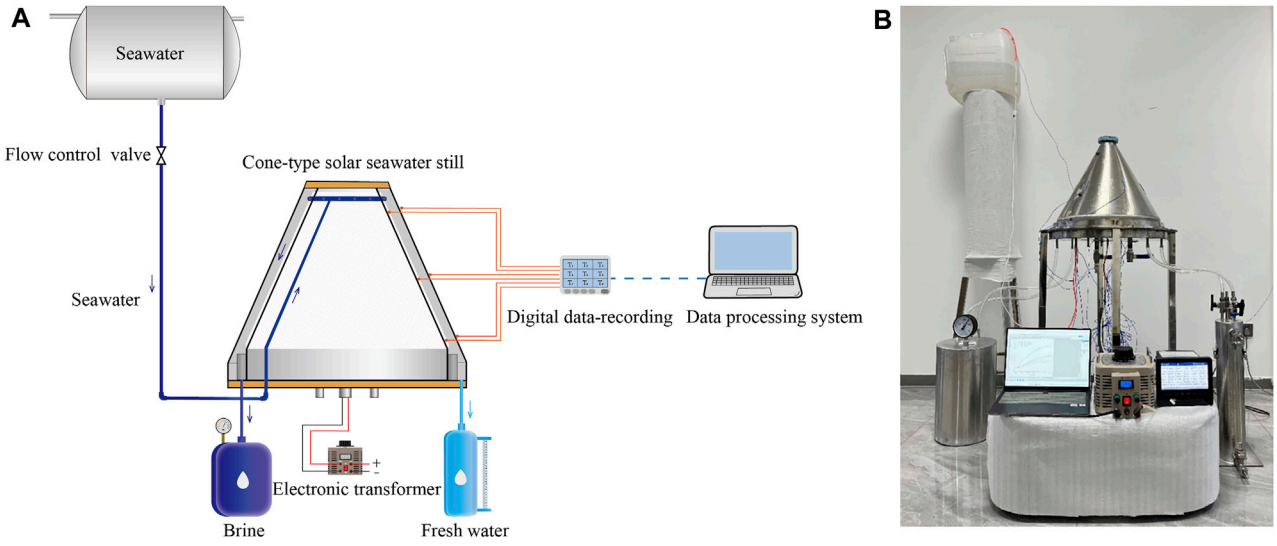

FIGURE 2
(A) Schematic of the test system. **(B)** Photograph of the experimental device.

TABLE 2 The parameters associated with the experimental devices.

Measuring device	Range	Accuracy	Standard uncertainty
20-channel digital data-recording	−35°C–300°C	±0.5%	±0.29%
Thermocouple	120°C–300°C	±0.5 °C	±0.29°C
Electronic transformer	0–250 V	±0.1%	±0.58%
Liquid level meter	0–360 mm	±0.5 mm	±0.29 mm
Thermal conductivity measuring instrument	0.03–12 W/(m·K)	±5%	±2.89%
Heat flow meter	0–±99990 W/m^2	±3%	±1.73%

To ensure the wetness of the evaporation surface to meet the design requirements, the wick material with moderate thickness and excellent moisture absorption performance should be selected and arranged on the evaporation surface. The wick material chosen for the CTSSS is two layers of skimmed cotton yarn in this study (Hou et al., 2018a).

To accurately measure the temperature of the evaporation surface and condensation surface, three thermocouples are arranged at the surfaces of the inner conical sleeve and the outer conical sleeve, respectively. Among them, the temperature in the middle of the conical sleeve is the evaporation temperature or condensation temperature of the CTSSS, and the temperature difference between the upper and lower parts of the inner or outer conical sleeve is taken as the vertical temperature difference of the evaporation or condensation, respectively. The ambient temperature is measured by another thermocouple placed far away from the test system. The thermocouple data is recorded by a 20–channel digital data recording at 1 min intervals, and the fresh water yield of the CTSSS is read from the liquid level meter at 20 min intervals. The parameters associated with the experimental devices are shown in Table 2.

2.3 Uncertainty

The comprehensive uncertainty u_C is used to analyze the uncertainty to verify the reliability of the test data, (Xu et al., 2021), the calculation formula is,

$$u_C(D) = \sqrt{u_A^2 + u_B^2} \tag{1}$$

where u_A is the type A uncertainty of multiple measurements, and u_B is the type B uncertainty of the measuring device and the calculation formulas are as follows (Rahbar and Asadi, 2016; Ahmed et al., 2022),

$$u_A = S(D) = \sqrt{\frac{\sum (D_i - D)^2}{k(k-1)}} \tag{2}$$

$$u_B = \frac{a}{\sqrt{3}} \tag{3}$$

where D_i is the measured value, D is the average value of measurements, k is the number of measurements, and a is the accuracy of the measuring device.

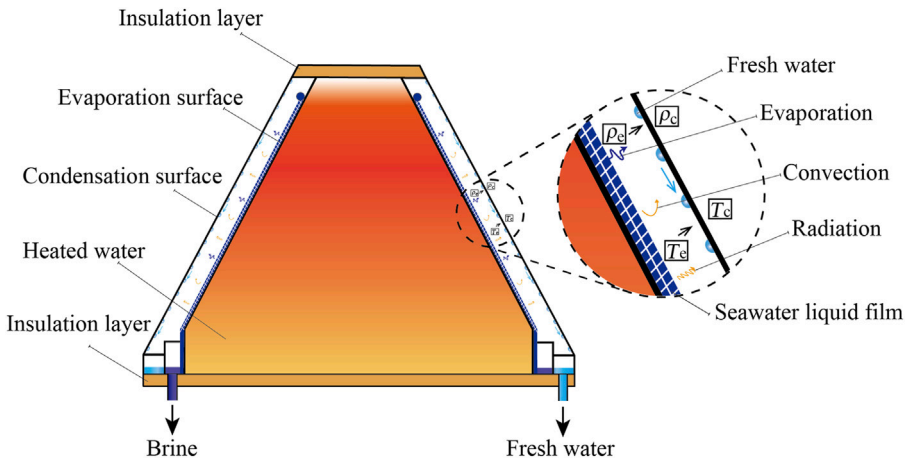

FIGURE 3
The heat and mass transfer of the CTSSS.

2.4 The heat and mass transfer in the cone-type solar seawater still

The heat and mass transfer of the binary mixed gas in the CTSSS is carried out in the annular enclosed small space between the two conical sleeves, and the process is shown in Figure 3. The seawater liquid film on the evaporation surface is heated and turns into water vapor during operation, which floats upward under the action of the water vapor temperature and density differences between the evaporation surface and condensation surface. The generated water vapor diffuses in the annular enclosed small space and condenses into the fresh water when it reaches the condensation surface with a lower temperature, meanwhile releasing the latent heat of vaporization. Simultaneously, the latent heat is released to the environment by convection and radiation through the condensation surface.

2.4.1 Mass transfer theory in the cone-type solar seawater still

As a parameter to evaluate the performance of the CTSSS, the fresh water yield depends on the evaporation area, mass transfer coefficient, and density difference between the evaporation surface and condensation surface. The theoretical calculation formula is,

$$m_w = A_e h_m (\rho_e - \rho_c) \tag{4}$$

where m_w is the fresh water yield per unit time of the CTSSS, kg/s; A_e is the evaporation area, m^2; h_m is the mass transfer coefficient, m/s; ρ_e and ρ_c are the densities of the binary mixed gas of evaporation surface and condensation surface, kg/m^3.

Based on the analog theory of heat and mass transfer, the h_m of the CTSSS depends on the convective heat transfer coefficient, and the theoretical formula is,

$$h_m = \frac{h_c D_{aw}}{k_m}\left(\frac{Sc}{Pr}\right)^n \tag{5}$$

where h_c is the convective heat transfer coefficient of the binary mixed gas, W/(m^2·K); k_m is the thermal conductivity of the binary mixed gas, W/(m·K); D_{aw} is the mass diffusion coefficient of the water vapor in the air, cm^2/s; Sc is the Schmidt number; Pr is the Prandtl number; n is the numerical constants and its value is 0.33 for the CTSSS (Tsilingiris, 2018). The formula of D_{aw} is,

$$D_{aw} = \frac{0.00143 T_m^{1.75}}{p_0 M_{aw}^{0.5}\left[(\sum_v)_a^{\frac{1}{3}} + (\sum_v)_w^{\frac{1}{3}}\right]^2} \tag{6}$$

$$M_{aw} = \frac{2}{\frac{1}{M_a} + \frac{1}{M_w}} \tag{7}$$

where T_m is the temperature of binary mixed gas, K; p_0 is the local atmospheric pressure, bar; $\sum_v$ is the molecular diffusion volume of each component in the binary mixed gas, and the subscripts a and w represent dry air and water vapor, respectively, and their values are 19.7 and 13.1 (Hou et al., 2018b), M is the average molar mass of binary mixed gas, g/mol; M_a and M_w are the molar mass of air and water vapor, g/mol. The calculation formulas of Sc and Pr are,

$$Sc = \frac{\mu_m}{D_{aw}\rho_m} \tag{8}$$

$$Pr = \frac{c_{p,m}\mu_m}{k_m} \tag{9}$$

where μ_m is the dynamic viscosity of binary mixed gas, Pa·s; ρ_m is the average density of binary mixed gas, kg/m^3; $c_{p,m}$ is the specific heat capacity of the binary mixed gas, J/(kg·K).

The h_c in the CTSSS mainly depends on the Rayleigh number, and the relationship between h_c and Ra is,

$$h_c = \frac{k_m C Ra^n}{L} \tag{10}$$

$$Ra = Gr \cdot Pr \tag{11}$$

where L is the characteristic size of the CTSSS, m; C and n are constants with values of 0.13 and 0.29 (Hou et al., 2018a), respectively; Gr and Pr are the Grashof number and the Prandtl number, respectively, and their formulas are,

$$Gr = \frac{gL^3\rho_m^2}{\mu_m^2 T_c}(T_e - T_c) \tag{12}$$

TABLE 3 The value of the coefficients of Eqs. 14–17.

Eq. 14	Equation 15	Equation 16	Equation 17
$A_0 = 1.299995662$	$B_0 = 1.088022802$	$C_0 = 1.685731754 \times 10^{-5}$	$D_0 = 0.02416826077$
$A_1 = -6.043625845 \times 10^{-3}$	$B_1 = -0.01057758092$	$C_1 = 9.151853945 \times 10^{-8}$	$D_1 = 5.526004579 \times 10^{-5}$
$A_2 = 4.697926602 \times 10^{-5}$	$B_2 = 4.769110559 \times 10^{-4}$	$C_2 = -2.16276222 \times 10^{-9}$	$D_2 = 4.631207189 \times 10^{-7}$
$A_3 = -5.760867827 \times 10^{-7}$	$B_3 = -7.898561559 \times 10^{-6}$	$C_3 = 3.413922553 \times 10^{-11}$	$D_3 = -9.489325324 \times 10^{-9}$
	$B_4 = 5.122303796 \times 10^{-8}$	$C_4 = -2.644372665 \times 10^{-13}$	

$$Pr = \frac{c_{p,m}\mu_m}{k_m} \tag{13}$$

where g is the local gravity, m/s^2; T_e is the evaporation temperature, K; T_c is the condensation temperature, K.

The binary mixed gas in the CTSSS is a mixture of dry air and water vapor. Both of them are considered ideal gases, and thermal physical parameters of the binary mixed gas can be calculated by (Tsilingiris, 2007),

$$\rho_m = A_0 + A_1 t + A_2 t^2 + A_3 t^3 \tag{14}$$

$$c_{p,m} = B_0 + B_1 t + B_2 t^2 + B_3 t^3 + B_4 t^4 \tag{15}$$

$$\mu_m = C_0 + C_1 t + C_2 t^2 + C_3 t^3 + C_4 t^4 \tag{16}$$

$$k_m = D_0 + D_1 t + D_2 t^2 + D_3 t^3 \tag{17}$$

where t is the temperature of binary mixed gas, ˚C; A_0–A_3, B_0–B_4, C_0–C_4, and D_0–D_3 are constants, and their values are shown in Table 3.

2.4.2 Heat transfer in the cone-type solar seawater still

The heat transfer of binary mixed gas mainly includes evaporation, convection, and radiation. Convective heat transfer and evaporative heat transfer are accompanied, which synchronously promote evaporation. Among these three kinds of heat, evaporative heat is used directly for the evaporation of water vapor, which significantly affects the performance of the CTSSS.

Ignoring the leakage of water vapor and the heat loss of the lower and upper bottom plates, the heat inputted to the CTSSS is all transmitted to the seawater liquid film and then transferred to the condensation surface by evaporation, convection, and radiation when the CTSSS is in steady state operation. The equations of evaporative, convective, and radiative heat transfer from evaporation surface to condensation surface are,

$$Q_{ew} = m_w h_{fg} \tag{18}$$

$$Q_{cw} = h_c A_e (T_e - T_c) \tag{19}$$

$$Q_{rw} = \frac{\sigma (T_e^4 - T_c^4) A_e}{\frac{1}{\varepsilon_e} + \frac{A_e}{A_c}\left(\frac{1}{\varepsilon_c} - 1\right)} \tag{20}$$

where Q_{ew}, Q_{cw} and Q_{rw} are the evaporative heat transfer, convective heat transfer, and radiative heat transfer of the evaporation surface, W; h_{fg} is the latent heat of water vaporization, J/kg; A_c is the condensation area, m^2; σ is the blackbody radiation constant with a value of 5.67×10^{-8} W/(m^2·K^4); ε_e and ε_c are the emissivities of evaporation surface and condensation surface, respectively. The emissivities of seawater liquid film, non-mirror condensation sleeve, and mirror condensation sleeve in this study are 0.96, 0.85 (Xie et al., 2018), and 0.09 (Woods et al., 2014), respectively.

It is approximately considered that the evaporation rate of water vapor is equal to the condensation rate. Therefore, the more significant the proportion of Q_{ew}, the greater the fresh water yield. The ratios of Q_{ew}, Q_{cw}, and Q_{rw} in the total heat transfer are,

$$R_e = \frac{Q_{ew}}{Q} \tag{21}$$

$$R_c = \frac{Q_{cw}}{Q} \tag{22}$$

$$R_r = \frac{Q_{rw}}{Q} \tag{23}$$

$$Q = Q_{ew} + Q_{cw} + Q_{rw} \tag{24}$$

where Q is the total heat transfer on the evaporation surface, W; R_e, R_c, and R_r are the proportion of Q_{ew}, Q_{cw}, and Q_{rw} in Q. When enhancing the mass transfer in the CTSSS, it can be achieved by increasing R_e and by reducing R_c and R_r.

2.4.3 The performance evaluation of the cone-type solar seawater still

The performance ratio (*PR*) can be used to define the thermal efficiency of the CTSSS for evaluating the thermal performance of the CTSSS, and the calculation formula is,

$$PR = \frac{m_w \cdot LH}{Q_{in}} \tag{25}$$

where *LH* is the latent heat of vaporization of water vapor, J/kg; Q_{in} is the heat energy inputted into the CTSSS, W. When the input power is the same, the larger the *PR*, the higher the fresh water yield and the better the thermal performance of the CTSSS.

3 Results and discussion

The test in this study includes two parts: rated heating power operation and rated heating temperature operation. Firstly, under the condition of constant power input, the fresh water yields of the CTSSS under different feed seawater mass flow rates were tested, and the influence mechanism of feed seawater mass flow rate on the performance of the CTSSS was clarified. Secondly, the influence of heating power and heating temperature on fresh water yields were tested during steady state operation at a constant temperature. Finally, the condensation sleeve was replaced by a mirror condensation sleeve to further improve the fresh water yield performance of the CTSSS and strengthen its mass transfer

TABLE 4 Parameters at steady state.

Input power (W)	Evaporation temperature (°C)	The temperature difference between evaporation and condensation (°C)	hm (m/s)	ρe −ρc (kg/m3)	Theorical fresh water yield (g/h)
200	80	6.5	0.005	0.0558	220

process. Then the variation curves of fresh water yield with heating temperature were obtained, and the proportions of heat transfer energy in the CTSSS with different condensation sleeves were analyzed.

3.1 Experiments under different feed seawater mass flow rates

The evaporation area, mass transfer coefficient, and density difference between evaporation and condensation surfaces directly affect the fresh water yield of the CTSSS, according to mass transfer theory. Among them, the evaporation area is affected by the wetting condition of the wick material. The evaporation area of the CTSSS is the wetting area of the wick material attached to the evaporation surface. The evaporation area reaches the maximum when the wick material is completely wetted, which is beneficial to the fresh water yield performance. The feed seawater mass flow rate is one of the main influence factors on the wetting condition of the wick material. When the feed seawater mass flow rate decreases, the wick materials at the bottom of the evaporation surface cannot be wetted entirely, and the actual evaporation area decreases, which is harmful to the fresh water yield. In addition, the feed seawater mass flow rate also affects the evaporation temperature. When the feed seawater mass flow rate is increased, the temperature of seawater liquid film on the evaporation surface is decreased, and the evaporation temperature is reduced, which has adverse effects on the fresh water yield of the CTSSS.

The fresh water yield of the CTSSS under different feed seawater mass flow rates was tested when the heating power is 200 W to explore the influence of the feed seawater mass flow rate on the CTSSS. According to the previous research (Li et al., 2023), when the heating power is 200 W, the temperatures of the CTSSS under steady state are shown in Table 4. By Eqs 4–17, the theorical h_m and $\rho_e - \rho_c$ are calculated, the fresh water yield is further obtained as 220 g/h. Then the fresh water yield of the CTSSS was tested when the feed seawater mass flow rates are 300 g/h and 400 g/h, under the condition that the feed seawater mass flow rate is greater than the fresh water yield. The heating power was kept constant at 200 W during the test, and the fresh water yield and temperature of the CTSSS with different feed seawater mass flow rates were obtained, as shown in Figure 4.

As can be seen from Figure 4, the CTSSS at different feed seawater mass flow rate conditions all experienced three stages: being heated, steady state operation and natural cooling. The time to reach steady state operation is prolonged with the increase in feed seawater mass flow rate. When the feed seawater mass flow rates are 300 g/h and 400 g/h, the durations for the CTSSS to reach steady state are 12 h 40 min and 14 h, respectively. The steady state evaporation temperature of the CTSSS is 80.1°C when the feed seawater mass flow rate is 400 g/h, which is 1.3°C lower than that when the feed seawater mass flow rate is 300 g/h. The reason behind this phenomenon can be explained as follows: when the feed seawater mass flow rate is increased, the heat demand for the same temperature rise of seawater liquid film is increased, the heating rate of the CTSSS is slowed down, then the heating duration of the CTSSS is extended and the evaporation temperature of seawater liquid film at the steady state is reduced.

Figure 4 shows that the fresh water yield of the CTSSS is consistent with the trend of its evaporation temperature. When the feed seawater mass flow rate is 400 g/h, the steady state fresh water yield is 62.8 g/20 min, which is 4.5% higher than that when the feed seawater mass flow rate is 300 g/h. This can be verified by the parameters of the CTSSS when it reaches the steady state, as shown in Table 5.

Table 5 presents that in the state of stable operation, when the feed seawater mass flow rate is increased from 300 to 400 g/h, the vertical temperature difference of the condensation surface is decreased by 1.9°C, the temperature difference between evaporation and condensation is increased by 0.9°C, and the *PR* is increased by 0.02. It can be considered that the mass transfer coefficients of the CTSSS are the same because the evaporation temperatures at the steady state under different feed seawater mass flow rates are approximately equal. The vertical temperature difference of the condensation surface is smaller when the feed seawater mass flow rate is 400 g/h compared with that when the feed seawater mass flow rate is 300 g/h. It indicates that the condensation and evaporation are more uniform, and the actual evaporation area is larger.

In addition, according to the thermophysical properties of the binary mixed gas, the density of the binary mixed gas near the evaporation surface and the condensation surface is a single-valued function of their temperatures. When the feed seawater mass flow rate is 400 g/h, the temperature difference between evaporation and condensation, and the density difference between the evaporation surface and condensation surface is larger, and the driving force of heat and mass transfer is stronger. Synthesize the above analysis, when the feed seawater mass flow rate is 400 g/h, the evaporation area and the density difference of the binary mixed gas near the evaporation surface and condensation surface is larger, the fresh water yield and the heat utilization efficiency of the CTSSS are higher, so the fresh water yield performance is better.

3.2 Experiments under different heating power

To further evaluate the energy utilization of the CTSS, the freshwater yield under different heating power was obtained by experiment. In the test, the feed seawater mass flow rate was 400 g/h, and the heating power was 180 W and 200 W respectively. The effect of heating power on the fresh water yield is depicted in Figure 5.

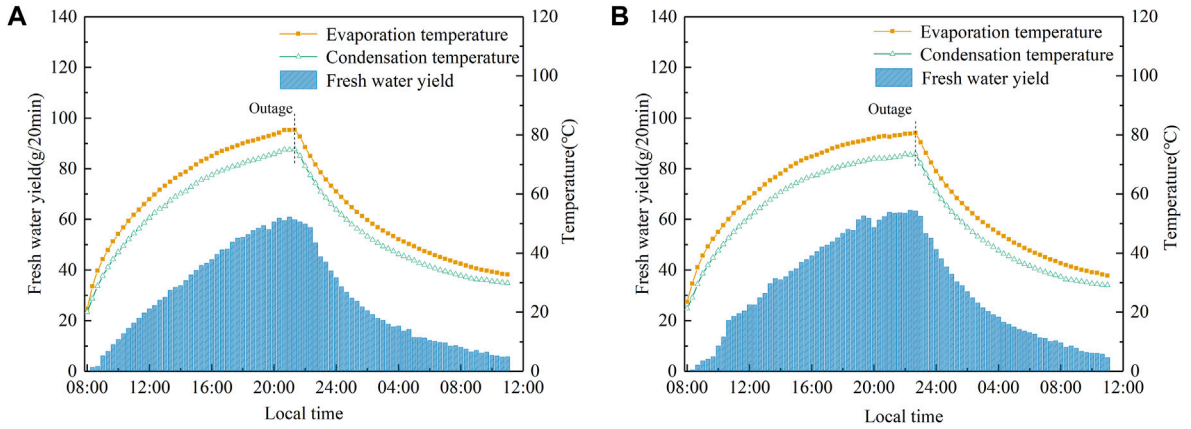

FIGURE 4
(A) Fresh water yields and temperatures of the CTSSS when the feed seawater mass flow rate is 300 g/h. **(B)** Fresh water yields and temperatures of the CTSSS when the feed seawater mass flow rate is 400 g/h.

TABLE 5 Parameters at steady state with different feed seawater mass flow rate.

Feed seawater mass flow rate (g/h)	Fresh water yield (kg/h)	Evaporation temperature (°C)	Condensation temperature (°C)	The vertical temperature difference of condensation surface (°C)	The average temperature difference between evaporation and condensation (°C)	*PR*
300	0.180	81.8	75.7	11.5	6.1	0.58
400	0.188	80.1	73.1	9.6	7.0	0.6

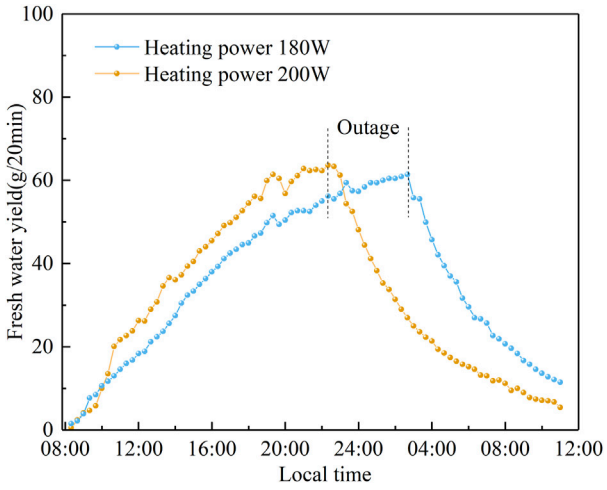

FIGURE 5
Fresh water yield with respect to local time at different heating power.

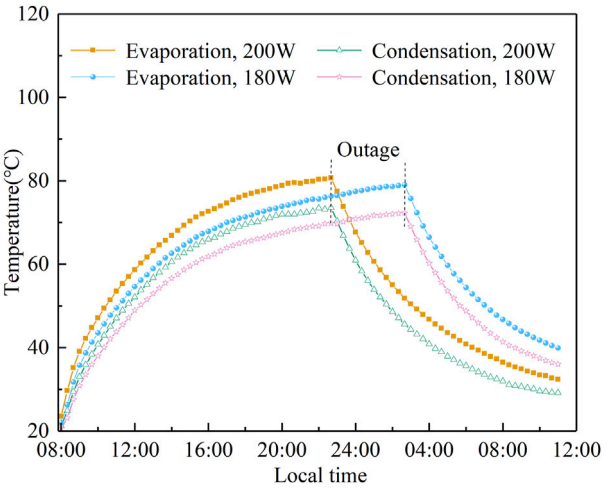

FIGURE 6
Evaporation temperature and condensation temperature variation with respect to local time at different heating power.

From Figure 5, it is clearly seen that the fresh water yield is increased gradually with the heating time, and it is dwindled rapidly after power outage. When 180 W heating power is employed, the fresh water yield is increased from 0.5 g/20 min to 60.7 g/20 min, and the steady state operation stage is achieved at 1:40. The fresh water yield is increased from 1.5 g/20 min to 62.8 g/20 min when the heating power is 200 W, and the time to reach the steady state operation stage is shifted to 21:00. At the being heated and steady state operation stage,

TABLE 6 Parameters at steady state with different input power.

Heating power (W)	Evaporation temperature (°C)	Condensation temperature (°C)	Fresh water yield (kg/h)	The average temperature difference between evaporation and condensation (°C)	PR
180	79.0	72.3	0.182	6.7	0.65
200	80.1	73.1	0.188	7.0	0.6

fresh water yield is smaller when the heating power is 180 W. The increase of fresh water yield with the increase of heating power can be explained by the evaporation temperature and condensation temperature variation trend of the CTSSS, as shown in Figure 6.

Figure 6 illustrates the temperature variation of both evaporation and condensation when the heating power is 180W and 200 W. It is observed that the evaporation temperature and condensation temperature increase gradually with the heating time. The CTSSS has a lower evaporation temperature when the heating power is 180 W compared with the other case, and noted as 79°C at the steady state operation stage. Due to the low evaporation temperature of the smaller heating power, the temperature difference between evaporation and condensation is smaller, which further hinder the improvement of fresh water yield. The parameters of the CTSSS at steady state are listed in Table 6.

From Table 6, it is very clear that the fresh water yield increase and the *PR* decreases as the input power increases. The reason is that when the heating power increases, the temperature of the CTSSS increases, and the temperature difference between the CTSSS and the environment increases, which leads a more heat loss and a lower energy utilization efficiency as well as the *PR*.

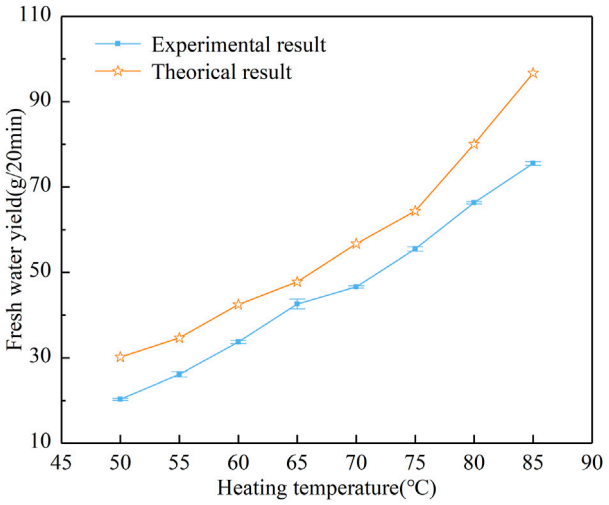

FIGURE 7
Comparison of the fresh water yield of predicted values and experimental values.

3.3 Experiments under different heating temperatures

The heat and mass transfer of the binary mixed gas in the CTSSS is mainly affected by the evaporation temperature. The higher the evaporation temperature, the greater the quality fraction of the water vapor among the binary mixed gas, the faster the corresponding evaporation rate. The fresh water yield at different heating temperatures was tested experimentally to explore the effect of heating temperature on the fresh water yield of the CTSSS. The heating temperature was set to 50°C–85°C referring to the operating temperature of the solar collector, and the temperature step was 5°C. The test began after the heating temperature reached the test temperature, and the running state reached the steady state and remained for 1 h. The test duration of each group was 1 h. The experimental results are obtained in Figure 7.

Figure 7 depicts the fresh water yield is increased as the heating temperature. When the heating temperature is 85°C, the fresh water yield is 75.5 g/20 min, which is 272% higher than that the heating temperature of 50°C. The partial pressure, mass transfer, and specific humidity of water vapor are improved with the increase of heating temperature, which further causes the enlargement of fresh water yield. What's more, the deviation between the fresh water yield of theoretical prediction and the experimental value is 10.84%–32.75%, which verified the suitability of the theoretical calculation methods of the CTSSS when the heating temperature is 50°C–85°C.

3.4 Performance improvement by replacing mirror condensation sleeve

It is beneficial that the heat capacity of seawater liquid film is small for accelerating the evaporation process. The small characteristic size of the CTSSS results in a short phase change heat transfer distance of the water vapor. As Equation 20 shows, reducing the emissivity of the condensation sleeve is conducive to reducing the radiative heat transfer and to increasing the evaporative heat transfer in the CTSSS. To reduce the emissivity of the condensation sleeve and explore the influence of the condensation sleeve on the mass transfer performance in the CTSSS, the non-mirror condensation sleeve and the mirror condensation sleeve were used in the test, and the photograph of them is shown in Figure 8, and the physical properties of the two condensation sleeves are listed in Table 7.

The fresh water yields of the CTSSS with non-mirror condensation sleeve and mirror condensation sleeve were tested in steady states, and the influence mechanism of condensation sleeve type on the performance of CTSSS was analyzed. The measured fresh water yield is shown in Figure 9.

Figure 9 indicates that the fresh water yield of the CTSSS with mirror condensation sleeve is higher than that with non-mirror condensation sleeve. When the heating temperature is 85°C, the fresh water yield of the CTSSS with mirror condensation sleeve is 84.6 g/20 min, which produced 12.1% more than the CTSSS with

FIGURE 8
Photograph of the non-mirror condensation sleeve and mirror condensation sleeve.

TABLE 7 Physical properties of the condensation sleeves.

Condensation sleeve	Roughness	Emissivity
Non-mirror condensation sleeve	1.6 um	0.85
Mirror condensation sleeve	0.1 um	0.09

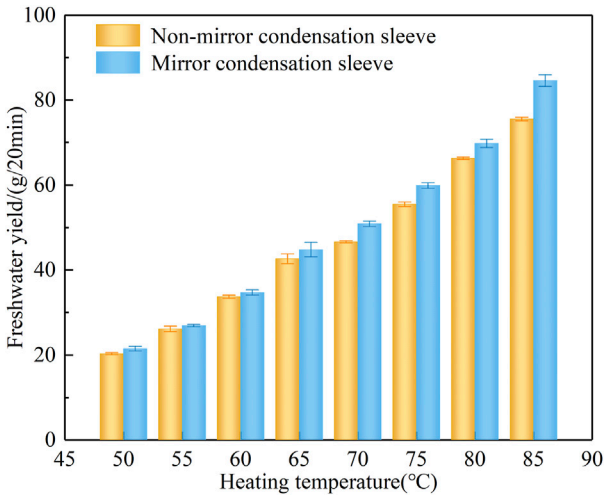

FIGURE 9
Variation of fresh water yield of the CTSSSs with different condensation sleeves.

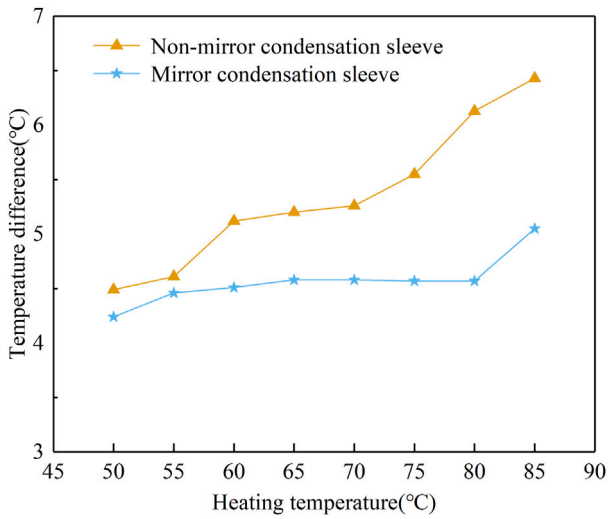

FIGURE 10
Variation of the temperature difference between evaporation and condensation of the CTSSSs with different condensation sleeves.

non-mirror condensation sleeve. This phenomenon can be explained by the temperature difference between evaporation and condensation of the CTSSS with different condensation sleeves, as shown in Figure 10.

As shown in Figure 10, the temperature difference between evaporation and condensation of the CTSSS with mirror condensation sleeve is smaller than that with non-mirror condensation sleeve. When the heating temperature is 85°C, the temperature difference between evaporation and condensation with mirror condensation sleeve is 5.1°C, which is 1.3°C lower than that with non-mirror condensation sleeve. The reason behind this phenomenon is that more water vapor condenses on mirror condensation sleeve, resulting in more latent heat release and higher condensation temperature. In addition, evaporative heat transfer is the main energy source for fresh water production in the CTSSS, so the mass transfer process in the still can be enhanced by increasing R_e and decreasing R_c and R_r. The R_e, R_c, and R_r in the CTSSS can be calculated by substituting the test evaporation temperature and condensation temperature into Equations 21–23. The calculation results are shown in Figure 11, that presents the variations in R_e, R_c, and R_r of CTSSS with non-mirror condensation

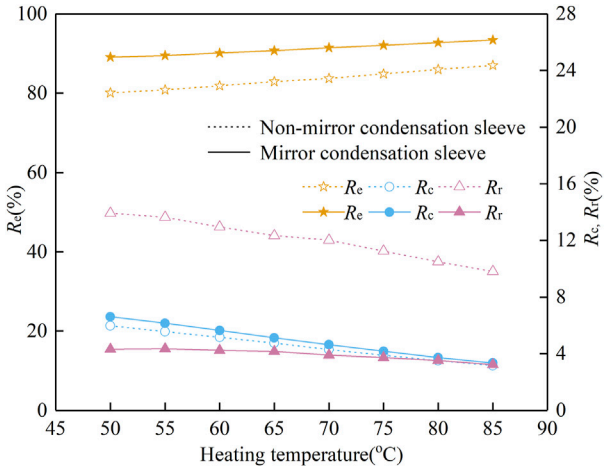

FIGURE 11
The proportion of evaporative, convective, and radiative heat transfer in the total heat transfer.

sleeve and mirror condensation sleeve concerning the heating temperature.

Figure 11 shows that the heat transfer in the CTSSS is dominated by evaporative heat transfer, and with the growth of heating temperature, R_e increased gradually, while the trend of R_c and R_r is opposite. R_e of CTSSS with non-mirror condensation sleeve is reached 87%, R_c and R_r are decreased to 3.2% and 9.8% when the heating temperature is 85°C. This indicates that the higher the heating temperature, the more significant the proportion of evaporative heat transfer and the better the thermal performance of the CTSSS.

When the heating temperature is 85°C, the value of R_r of the CTSSS with mirror condensation sleeve is 3.2%, which is 6.6% lower than that of the CTSSS with non-mirror condensation sleeve. Meanwhile, the value of R_e and R_c of the CTSSS with mirror condensation sleeve are 93.4% and 3.4%, respectively, higher than that with non-mirror condensation sleeve. This indicates that the radiative heat transfer in the CTSSS with mirror condensation sleeve is weakened and mainly converted into evaporative heat transfer, which is also one of the reasons for improving the performance of the CTSSS with mirror condensation sleeve.

4 Conclusion

In this study, a novel CTSSS was designed with the evaporation surface and condensation surface paralleled each other, which has the characteristics of a large condensation area, short mass transfer distance, and small heat transfer resistance. Tests were carried out under the condition of constant heating power and temperature to explore the performance of the CTSSS in the laboratory. Through experimental investigation and theoretical analysis, the following conclusions are obtained:

(1) The steady state fresh water yield of the CTSSS was 62.7g/20 min when the feed seawater mass flow rate and heating power were 400 g/h and 200 W, respectively, which is 4.5% higher than that when the feed seawater mass flow rate was 300 g/h.
(2) The evaporation temperature and temperature difference between evaporation and condensation are increased as the heating power, as well as the fresh water yield and *PR*. When 180 W heating power is employed, the *PR* of the CTSSS is 0.65, which is 0.05 higher than that when the heating power is 200 W.
(3) The fresh water yield of the CTSSS was augmented as the increase of heating temperature. When the heating temperature was 85°C, the fresh water yields of the CTSS with mirror condensation sleeve and non-mirror condensation sleeve were 84.6 g/20 min and 75.5 g/20 min, respectively. The fresh water yield is increased by 12.1% after replacing the mirror condensation sleeve.
(4) In contrast to the CTSSS with non-mirror condensation sleeve, the radiative heat transfer is weakened, and the evaporative heat transfer is strengthened in the CTSSS with mirror condensation sleeve compared to the CTSSS with non-mirror condensation sleeve. The value of R_r and R_e of the CTSSS with mirror condensation sleeve were decreased by 6.6% and increased by 6.4% than that with non-mirror condensation sleeve.

Data availability statement

The original contributions presented in the study are included in the article/supplementary material, further inquiries can be directed to the corresponding author.

Author contributions

JY: Conceptualization, Methodology, Validation, Writing–original draft. ZC: Conceptualization, Data curation, Funding acquisition, Methodology, Writing–review and editing. XZ: Formal Analysis, Methodology, Validation, Writing–original draft. GZ: Formal Analysis, Software, Writing–review and editing.

Funding

The author(s) declare financial support was received for the research, authorship, and/or publication of this article. We gratefully acknowledge the financial support for this research provided by the National Natural Science Foundation of China (No. 51966012) Projects, Program for Innovative Research Team in Universities of Inner Mongolia Autonomous Region (NMGIRT2404), Key R&D and Achievement Transformation Plan of Inner Mongolia Autonomous Region (No. 2022YFXZ0021), Central Government Guiding Local Science and Technology Development Funds (No. 2022ZY0085).

Conflict of interest

The authors declare that the research was conducted in the absence of any commercial or financial relationships that could be construed as a potential conflict of interest.

Publisher's note

References

Abou-Shady, A., and El-Araby, H. (2021). Electro-agric, a novel environmental engineering perspective to overcome the global water crisis via marginal water reuse. *Nat. Hazards Res.* 1, 202–226. doi:10.1016/j.nhres.2021.10.004

Abujazar, M. S. S., Fatihah, S., Ibrahim, I. A., Kabeel, A., and Sharil, S. (2018). Productivity modelling of a developed inclined stepped solar still system based on actual performance and using a cascaded forward neural network model. *J. Clean. Prod.* 170, 147–159. doi:10.1016/j.jclepro.2017.09.092

Ahmed, M. M. Z., Alshammari, F., Abdullah, A. S., and Elashmawy, M. (2021a). Basin and tubular solar distillation systems: a review. *Process Saf. Environ.* 150, 157–178. doi:10.1016/j.psep.2021.04.015

Ahmed, M. M. Z., Alshammari, F., Abdullah, A. S., and Elashmawy, M. (2021b). Enhancing tubular solar still performance using double effect with direct sunrays concentration. *Sol. Energy Mat. Sol. C* 230, 111214. doi:10.1016/j.solmat.2021.111214

Ahmed, M. M. Z., Alshammari, F., Alatawi, I., Alhadri, M., and Elashmawy, M. (2022). A novel solar desalination system integrating inclined and tubular solar still with parabolic concentrator. *Appl. Therm. Eng.* 213, 118665. doi:10.1016/j.applthermaleng.2022.118665

Arunkumar, T., Wang, J., and Denkenberger, D. (2021). Capillary flow-driven efficient nanomaterials for seawater desalination: review of classifications, challenges, and future perspectives. *Renew. Sustain. Energy Rev.* 138, 110547. doi:10.1016/j.rser.2020.110547

Chandrashekara, M., and Yadav, A. (2017). Water desalination system using solar heat: a review. *Renew. Sustain. Energy. Rev.* 67, 1308–1330. doi:10.1016/j.rser.2016.08.058

Chang, Z., Zheng, Y., Chen, Z., Zheng, H., ZhaoSu, M. Y., and Mao, J. (2015). Performance analysis and experimental comparison of three operational modes of a triple-effect vertical concentric tubular solar desalination device. *Desalination* 375, 10–20. doi:10.1016/j.desal.2015.07.020

Choong, W. S., Ho, Z. Y., and Bahar, R. (2020). Solar desalination using fresnel lens as concentrated solar power device: an experimental study in tropical climate. *Front. Energy Res.* 8, 565542. doi:10.3389/fenrg.2020.565542

Elashmawy, M., Alhadri, M., and Ahmed, M. M. Z. (2021). Enhancing tubular solar still performance using novel PCM-tubes. *Desalination* 500, 114880. doi:10.1016/j.desal.2020.114880

Essa, F. A., Abdullah, A. S., and Omara, Z. M. (2021). Improving the performance of tubular solar still using rotating drum – experimental and theoretical investigation. *Process Saf. Environ.* 148, 579–589. doi:10.1016/j.psep.2020.11.039

Hou, J., Yang, J., Chang, Z., Zheng, H., and Su, Y. (2018a). The mass transfer coefficient assessment and productivity enhancement of a vertical tubular solar brackish water still. *Appl. Therm. Eng.* 128, 1446–1455. doi:10.1016/j.applthermaleng.2017.09.129

Hou, J., Yang, J., Chang, Z., Zheng, H., and Su, Y. (2018b). Effect of different carrier gases on productivity enhancement of a novel multi-effect vertical concentric tubular solar brackish water desalination device. *Desalination* 432, 72–80. doi:10.1016/j.desal.2018.01.011

Jafaripour, M., Roghabadi, F. A., Soleimanpour, S., and Sadrameli, S. M. (2023). Barriers to implementation of phase change materials within solar desalination units: exergy, thermal conductivity, economic, and environmental aspects review. *Desalination* 546, 116191. doi:10.1016/j.desal.2022.116191

Kabeel, A. E., Harby, K., Abdelgaied, M., and Eisa, A. (2021). Performance improvement of a tubular solar still using V-corrugated absorber with wick materials: numerical and experimental investigations. *Sol. Energy* 217, 187–199. doi:10.1016/j.solener.2021.02.008

Li, H., Chang, Z., Hou, J., Zhang, X., and Zhu, G. (2023). Experimental study on cone-type falling film evaporation solar brackish water desalination devices. *Renew. Energy Resour.* 41, 193–198. doi:10.19912/j.0254-0096.2020.08.035

Li, R., Zhu, G., Hou, J., Chang, Z., Li, Y., and Liu, Y. (2020). Effect of characteristic size on performance of vertical tubular falling film evaporation solar seawater distillation device. *Acta Energiae Solaris Sin.* 41, 258–263.

Nagaraju, V., Murali, G., Bewoor, A. K., Kumar, R., Sharifpur, M., Assad, M. E. H., et al. (2022). Experimental study on performance of single slope solar still integrated with sand troughs. *Sustain. Energy Technol. Assessments* 50, 101884. doi:10.1016/j.seta.2021.101884

Rahbar, N., and Asadi, A. (2016). Solar intensity measurement using a thermoelectric module; experimental study and mathematical modeling. *Energy Convers. Manag.* 129, 344–353. doi:10.1016/j.enconman.2016.10.007

Sangeetha, A., Shanmugan, S., and Gorjian, S. (2022). Experimental evaluation and thermodynamic Gibbs free energy analysis of a double-slope U-shaped stepped basin solar still using activated carbon with ZnO nanoparticles. *J. Clean. Prod.* 380, 135118. doi:10.1016/j.jclepro.2022.135118

Sharshir, S. W., Kandeal, A. W., Ellakany, Y. M., Maher, I., Khalil, A., Swidan, A., et al. (2022). Improving the performance of tubular solar still integrated with drilled carbonized wood and carbon black thin film evaporation. *Sol. Energy* 233, 504–514. doi:10.1016/j.solener.2022.01.065

Srithar, K., and Rajaseenivasan, T. (2018). Recent fresh water augmentation techniques in solar still and HDH desalination – a review. *Renew. Sustain. Energy. Rev.* 82, 629–644. doi:10.1016/j.rser.2017.09.056

Tiwari, G. N., and Kumar, A. (1988). Nocturnal water production by tubular solar stills using waste heat to preheat brine. *Desalination* 69, 309–318. doi:10.1016/0011-9164(88)80032-8

Tsilingiris, P. T. (2007). The influence of binary mixture thermophysical properties in the analysis of heat and mass transfer processes in solar distillation systems. *Sol. Energy* 81, 1482–1491. doi:10.1016/j.solener.2007.02.005

Tsilingiris, P. T. (2018). Modeling heat and mass transport phenomena at higher temperatures in solar distillation systems – the Chilton–Colburn analogy. *Sol. Energy* 84, 308–317. doi:10.1016/j.solener.2009.11.012

Wang, J., and Huo, E. (2022). Opportunities and challenges of seawater desalination technology. *Front. Energy Res.* 10, 960537. doi:10.3389/fenrg.2022.960537

Wang, M., Wei, Y., WangLi, X. R., Zhang, S., Wang, K., Wang, R., et al. (2023). An integrated system with functions of solar desalination, power generation and crop irrigation. *Nat. Water* 1, 716–724. doi:10.1038/s44221-023-00118-0

Woods, S. I., Jung, T. M., Sears, D. R., and Yu, J. (2014). Emissivity of silver and stainless steel from 80 K to 300 K: Application to ITER thermal shields. *Cryogenics* 60, 44–48. doi:10.1016/j.cryogenics.2014.01.002

Xie, G., Sun, L., Yan, T., Tang, J., Bao, J., and Du, M. (2018). Model development and experimental verification for tubular solar still operating under vacuum condition. *Energy* 157, 115–130. doi:10.1016/j.energy.2018.05.130

Xu, J., Chen, F., and Deng, C. (2021). Design and analysis of a novel multi-sectioned compound parabolic concentrator with multi-objective genetic algorithm. *Energy* 225, 120216. doi:10.1016/j.energy.2021.120216

Yan, T., Xie, G., Chen, W., Wu, Z., Xu, J., and Liu, Y. (2021). Experimental study on three-effect tubular solar still under vacuum and immersion cooling. *Desalination* 515, 115211. doi:10.1016/j.desal.2021.115211

Yang, Y., Feng, H., Que, W., Qiu, Y., Li, Y., Guo, L., et al. (2023). A diode-like scalable asymmetric solar evaporator with ultra-high salt resistance. *Adv. Funct. Mat.* 33, 2210972. doi:10.1002/adfm.202210972

Yeang, J. Y. K., Bahar, R., Koo, C. H., and Lee, S. S. (2023). Performance evaluation of a multi-stage solar distiller associated with Fresnel lens in Malaysian weather. *Front. Energy Res.* 11, 1137941. doi:10.3389/fenrg.2023.1137941